Wear 572–573 (2025) 206040

Contents lists available at ScienceDirect

Wear

journal homepage: www.elsevier.com/locate/wear

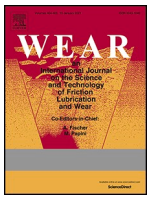

A case study on extended approach for wear analysis of TiAlCrSiN coated cutting inserts

K. Bobzin [a], C. Kalscheuer [a], M. Tayyab [a,*], T. Bergs [b], M. Meurer [b], M. Abouridouane [b]

[a] Surface Engineering Institute, RWTH Aachen University, Kackertstraße 15, 52072, Aachen, Germany
[b] Manufacturing Technology Institute, RWTH Aachen University, Campus-Boulevard 30, 52074, Aachen, Germany

ARTICLE INFO

Keywords:
PVD
TiAlCrSiN
Tool wear
Wear mechanisms
Nanocomposite
High performance
Cutting

ABSTRACT

There is an increasing demand for physical vapor deposition nanocomposite tool coatings such as TiAlCrSiN for challenging cutting operations. Here, a holistic data-driven modeling approach including coating properties, thermomechanical tool loading, comprehensive tool wear analysis and cutting process data is required for coated tool qualification. Hence, current study focuses on development of an extended tool wear analysis approach for TiAlCrSiN coated cemented carbide inserts required for model-based qualification of such tools. Monolayer TiAlCrSiN and bilayer TiAlCrSiON/TiAlCrSiN coatings were deposited on cemented carbide inserts and characterized. The wear behavior of coated variants was studied during dry turning of quenched and tempered 42CrMo4+QT alloy steel. In addition to VB measurement, an image analysis algorithm was developed to quantify the extended tool wear features with SEM images. Monolayer TiAlCrSiN, due to its higher temperature-dependent indentation hardness H_{IT}, displayed higher abrasive wear resistance. The oxynitride top layer for bilayer variant reduced the workpiece material adhesion to the tool rake face and resultantly improved crater wear resistance of the inserts. Moreover, the qualitative observations on tool wear behavior were validated with quantitative evaluation of tool wear features and process forces. The study implemented initial steps to realize an extended quantitative tool wear analysis approach for improved understanding on wear development in PVD-coated cutting tools.

1. Introduction

Productivity of cutting processes represents an important aspect for economic viability of manufacturing components for industrial applications. Here, tool life and choice of cutting parameters may contribute to the productivity improvement of cutting processes. Wear resistant physical vapor deposition (PVD) coatings are one of the established solutions to improve the service life of cutting tools [1]. However, with increasing demand for productivity improvement and development of difficult to cut materials, the cutting parameters are becoming more challenging, giving rise to high performance cutting processes. This has led to an increased demand of advanced wear resistant coating systems for such cutting operations. Here, the nanocomposite coating systems such as TiSiN, TiAlSiN, CrAlSiN and TiAlCrSiN represent promising wear reduction solutions for cutting tools. Si is known to restrict the growth of (Ti, Al, Cr)N grains by forming amorphous Si_3N_4 matrix, resulting in a nanocomposite structure [2]. Inclusion of Al gives the coating an increased oxidation resistance and hardness compared to binary CrN or TiN [3]. Due to the reduced grain size as well as the high cohesive strength between the nanograins and the amorphous matrix, the nanocomposite coatings exhibit superior hardness and crack resistance compared to polycrystalline coating systems with a comparable chemical composition [2,4]. In addition, the amorphous Si_3N_4 matrix may inhibit the diffusion processes at the grain boundaries to increase the oxidation resistance and thermal stability of the nanocomposite coatings [5,6]. However, the advantageous properties of such coatings may depend on the size of nanograins and of Si-based amorphous content [7–9]. The improved thermomechanical properties of the nanocomposite coatings may result in higher service life of coated tools during challenging cutting processes [10,11]. For this purpose, TiAlCrSiN represents an advanced nanocomposite coating system to potentially combine the individual advantages of Al, Cr and Si addition to TiN matrix in a single coating [12]. The, incorporation of oxygen in nitride hard coatings has shown promising potential to reduce adhesion of steel workpiece material on coated cutting tool [13]. However, the oxygen incorporation in TiAlCrSiN may increase the amorphous content of the

* Corresponding author.
E-mail address: tayyab@iot.rwth-aachen.de (M. Tayyab).

https://doi.org/10.1016/j.wear.2025.206040
Received 19 November 2024; Received in revised form 13 March 2025; Accepted 18 March 2025
Available online 18 March 2025

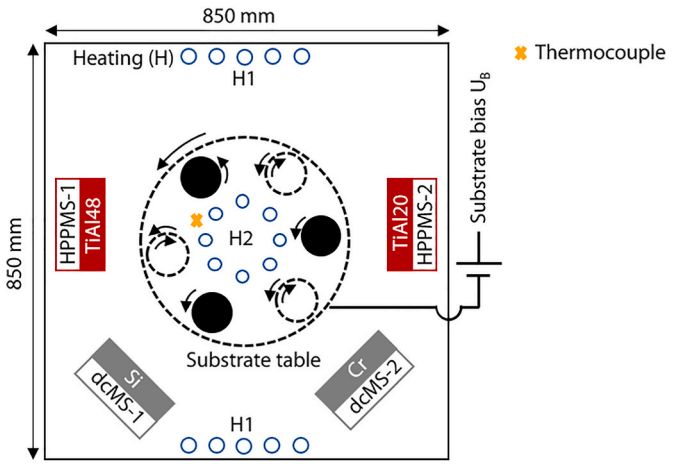

Fig. 1. Schematic of coating chamber of industrial coating unit CC800/9 HPPMS.

Table 1
Process parameters used for deposition of investigated coatings.

Coating process	Monolayer TiACrSiN	Bilayer TiAlCrSiON/TiAlCrSiN
Sample ID/-	5006	5007
Pressure p/mPa	520	520
Argon flow $Q(Ar)$/sccm	200	200
Nitrogen flow $Q(N_2)$/sccm	Pressure controlled	Pressure controlled
Oxygen flow $Q(O_2)$/sccm	–	18
Heating power P_H/kW	8	8
Heating power in middle P_{H2}/kW	4	4
Maximum coating temperature T_{max}/°C	590	590
Substrate bias U_B/V	−80	−80
Average power of HPPMS cathodes P_{HPPMS}/kW	7	7
Power dcMS-1 $P_{dcMS\text{-}1}$/kW	0.6	0.6
Power dcMS-2 $P_{dcMS\text{-}2}$/kW	0.3	0.3
Pulse frequency f/Hz	2000	2000
Pulse duration t_{on}/µs	60	60
Coating time TiAlCrN-Bond layer $t_{TiAlCrN}$/s	5400	5400
Coating time TiAlCrSiN $t_{TiAlCrSiN}$/s	14,500	10,400
Coating time TiAlCrSiON $t_{TiAlCrSiON}$/s	–	4800

resulting TiAlCrSiON coating and reduce the wear resistance of the coated tool [12]. The advantages of oxygen incorporation can potentially be combined with that of TiAlCrSiN in a bilayer coating architecture with nitride interlayer and an oxynitride top layer.

As the wear process of coated tools is an intricate system of interrelated physical processes, the qualification of advanced nanocomposite tool coatings, such as TiAlCrSiN, for high performance cutting operations requires cost and time intensive experimental efforts. Analytical models [14] and numerical simulation models [15] may provide useful information on thermomechanical tool load. However, these models are mostly based on simplified boundary conditions and largely ignore the effect of coating on wear mechanisms and tool wear behavior. In last few years, machine learning based data-driven models have shown encouraging results in terms of tool wear prediction for considered scenarios [16,17]. However, their robustness is associated with uncertainties when it comes to changing boundary conditions. Moreover, these models are mostly based on cutting process data and limited information on tool wear behavior in terms of flank wear land width measurements VB. The robustness of data-driven models can be improved through greybox-modelling approach [18,19]. Greybox models couple the analytical or simulation-based information with data-driven models. In order to develop such grey box models for accurate tool wear prediction, a comprehensive data-set containing information on coating properties, thermomechanical tool loading, cutting process data and detailed analysis of tool wear behavior is required. Currently, wear analysis of coated tools is mostly comprising of VB measurements and qualitative observations on underlying wear mechanisms based on scanning (SEM) or transmission electron microscopy (TEM) images of worn out tools. Hence, current study presents an extended tool wear analysis approach for nanocomposite TiAlCrSiN coated cemented carbide inserts, which may contribute to the development of wear prediction models for

Table 2
Coating thickness s, average line roughness Ra, chemical composition and adhesion strength class HF of monolayer TiAlCrSiN and bilayer TiAlCrSiON/TiAlCrSiN.

Coating	Monolayer TiACrSiN	Bilayer TiAlCrSiON/TiAlCrSiN
s/µm	2.8	2.6
Ra/µm	0.08	0.08
Ti/at.%	17	16
Al/at.%	25	23
Cr/at. %	3	<1
Si/at. %	2	1
O/at. %	<1	30
N/at. %	53	30
HF/-	1	1

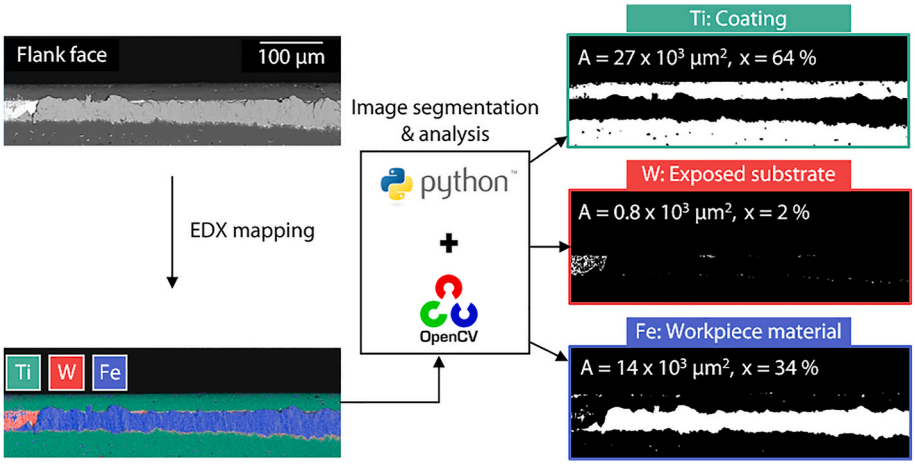

Fig. 2. Schematic representation of the approach used for quantitative analysis of tool wear features.

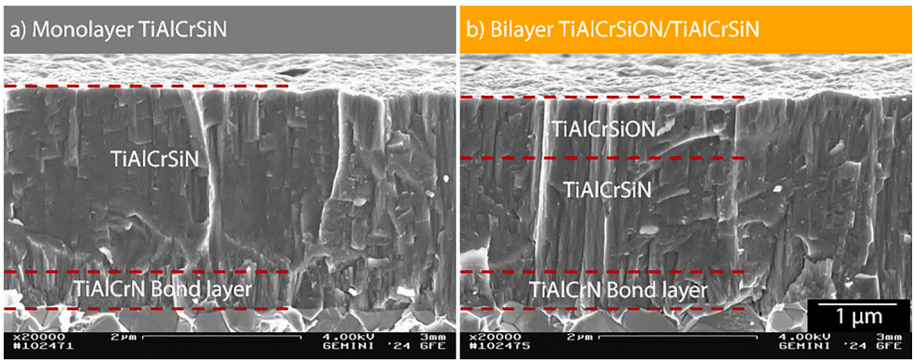

Fig. 3. SEM cross-section images of (a) monolayer TiAlCrSiN and (b) bilayer TiAlCrSiON/TiAlCrSiN.

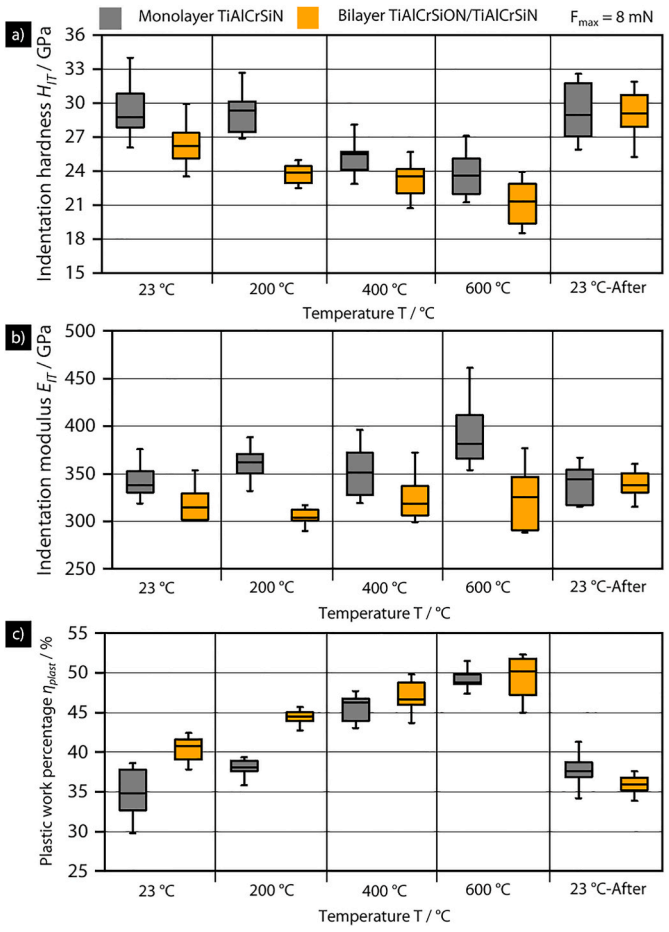

Fig. 4. Temperature dependent (a) indentation hardness H_{IT}, (b) indentation modulus E_{IT} and (c) plastic work percentage η_{plast} of monolayer and bilayer variants.

qualification of such tools. The wear behavior of cemented carbide inserts coated with monolayer TiAlCrSiN and bilayer TiAlCrSiON/-TiAlCrSiN is investigated during high performance cutting of quenched and tempered 42CrMo4+QT alloy steel. The effect of oxynitride TiAlCrSiON top layer on wear behavior of coated inserts is qualitatively understood and quantitatively validated using the extended tool wear analysis approach.

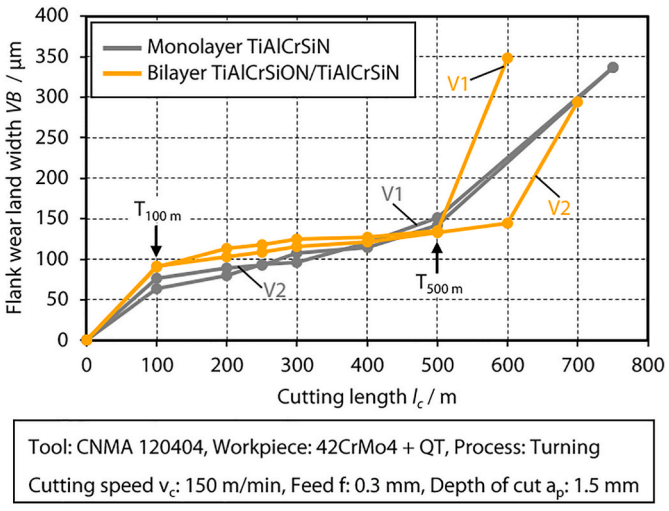

Fig. 5. Flank wear land width VB for cutting inserts coated with monolayer TiAlCrSiN and bilayer TiAlCrSiON/TiAlCrSiN from cuttings tests.

2. Experimental methods

2.1. Coating deposition

Cemented carbide inserts SNUN 120412 and CNMA 120404, ISO code K20-K40 and grade CTS18D, CERATIZIT Luxembourg S.á.r.l, Mamer, Luxembourg, were coated with monolayer TiAlCrSiN and bilayer TiAlCrSiN/TiAlCrSiON. An industrial PVD unit CC800/9 HPPMS, CemeCon AG, Wuerseln, Germany, was used for this purpose. Both coatings were deposited using same target configuration, see Fig. 1. TiAl48 and TiAl20 targets having 40 and 20 Al plugs, respectively, were installed on high power pulse magnetron sputtering (HPPMS) cathodes. Direct current magnetron sputtering (dcMS) cathodes were operated with pure Si and Cr targets. The temperature inside the coating chamber was measured by placing a K-Type thermocouple at the location shown in Fig. 1.

The process parameters from both coating variants are shown in Table 1. As apparent from cathode powers, the coatings were designed to have a high HPPMS content. The coating process of monolayer TiAlCrSiN was used as the basis for bilayer variant. For TiAlCrSiON top layer, oxygen with a flowrate $Q(O_2) = 18$ sccm was introduced after deposition of TiAlCrSiN interlayer. The coating time for TiAlCrSiON was adjusted to achieve a comparable overall coating thickness for both variants. During coating, the samples were subjected to three-fold rotation with table speed $n_{Table} = 2.5\ min^{-1}$.

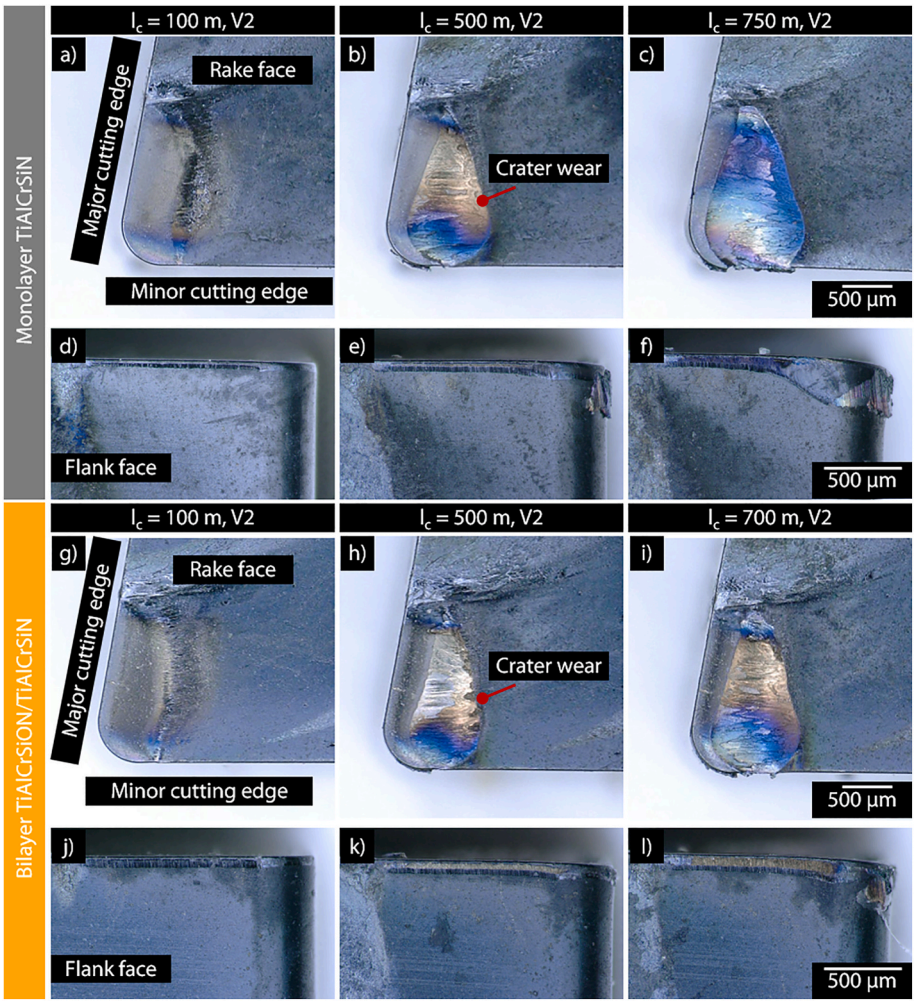

Fig. 6. Wear on flank and rake face of (a–f) TiAlCrSiN and (g–l) TiAlCrSiON/TiAlCrSiN coated cutting inserts at varying cutting lengths l_c over the tool service life.

2.2. Coating and compound characterization

Coating morphology and thickness were analyzed using SEM images of coating cross-section. For this purpose, Zeiss DSM 982 Gemini, Carl Zeiss AG, Oberkochen, Germany, was used. Chemical composition of the coatings was determined by electron probe microanalysis (EPMA) using JEOL JXA-8530, JEOL Ltd., Tokyo, Japan. SEM and EPMA investigations were carried out at Central Facility for Electron Microscopy (GFE), RWTH Aachen University, Aachen, Germany. Confocal laser scanning microscope (CLSM), Keyence VK-X210, Tokyo, Japan, was used to measure the average line roughness Ra. The elastic-plastic deformation behavior of the coatings was studied with nanoindentation. Here, measurements were carried out at T = 23 °C, T = 200 °C, T = 400 °C and T = 600 °C as well as at T = 23 °C after cooling down the sample. A TriboIndenter TI 950 equipped with xSol 25 high temperature stage, Bruker Corporation, Billerica, Massachusetts, USA, was used for high temperature nanoindentation measurements. The samples were placed between two heating plates which were equipped with heating elements, thermocouples, insulators and water-cooling channels. The temperature during the measurements was controlled by a PID controller. A Berkovich shaped diamond indenter tip with nominal radius r ≈ 150 nm was used for measurements. For each sample variant and temperature, 15 measurements with maximum indentation force F = 8 mN were carried out. The indenter tip was air-cooled during the measurements. Moreover, forming gas 95 % N_2 + 5 % H_2 was purged between the heating plates to achieve a protected atmosphere for the sample as well as the indenter. This also helped to minimize wear of the indenter tip at increased temperatures. The wear of the indenter tip was monitored through additional indentations on polycarbonate sample before and after high temperature measurements. In present case, no significant wear of the indenter tip was observed. Indentation hardness H_{IT} and indentation modulus E_{IT} were calculated from measurement data as per the method suggested by Oliver and Pharr [20]. As commonly known for ceramic coatings, Poisson's ratio ν = 0.25 was used for calculations. The adhesion between coating and substrate was measured at rake and flank face of coated CNMA 120404 inserts as per DIN 4856 Rockwell C indentation method. The tests with a normal force F ≈ 588.4 N were carried out using diamond indenter with cone angle Θ = 120° installed on HP100 Rockwell tester, KNUTH Machine Tools GmbH, Wasbek, Germany. Afterwards, the indents were analyzed by CLSM to determine the adhesion strength class (HF).

2.3. Cutting tests

For cutting tests, cemented carbide inserts CNMA 120404, ISO code K20-K40, grade CTS18D, CERATIZIT Luxembourg S.á.r.l, Mamer, Luxembourg, were coated as mentioned in section 2.1. The cutting inserts had a wedge angle β = 80° and corner radius r_ε = 0.4 mm. In order to investigate the wear behavior of the coated inserts, CNC longitudinal turning of quenched and tempered 42CrMo4+QT alloy steel was performed using DMG MORI NEF 600, DMG MORI AG, Bielefeld, Germany. The cutting tests were carried out in dry condition with the cutting speed v_c = 150 m/min, the depth of cut a_p = 1.5 mm and the feed f = 0.3 mm. These cutting parameters were determined based on tool manufacturer

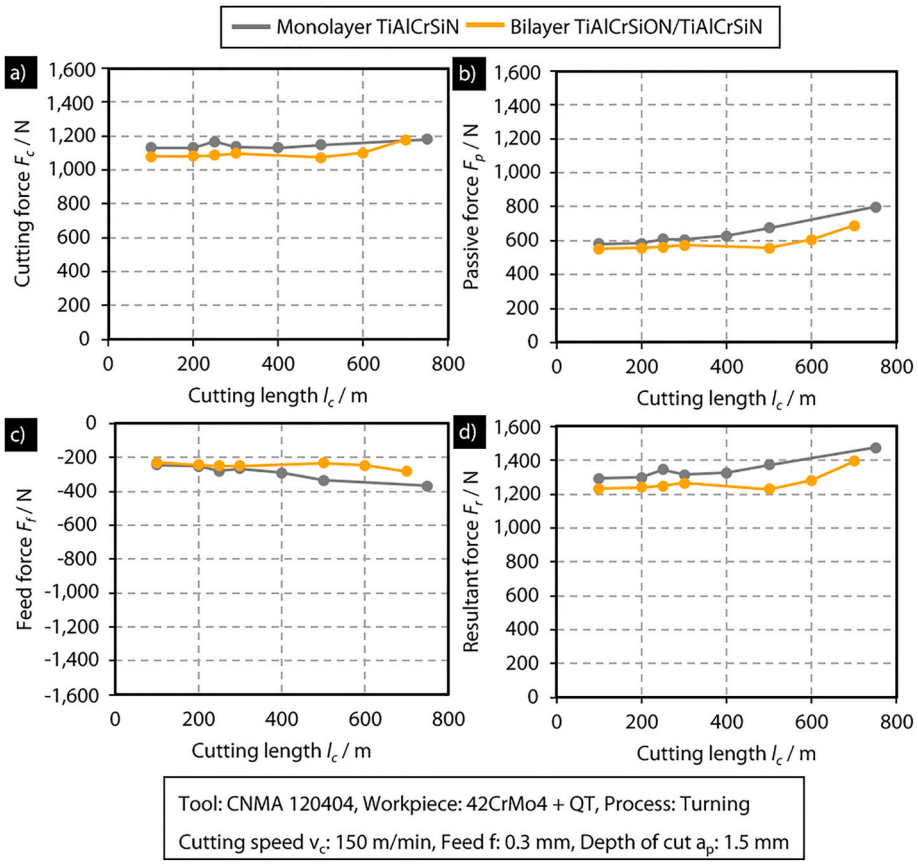

Fig. 7. Fig. 7: (a) Cutting force F_c, (b) passive force F_p, (c) feed force F_f and (d) resultant force F_r of TiAlCrSiN and TiAlCrSiON/TiAlCrSiN coated cutting inserts at varying cutting lengths l_c over the tool service life.

recommendations and preliminary turning tests. The evaluation of tool life was made by flank wear land width VB measurements after regular cutting length intervals. Maximum flank wear land width $VB_{max} = 250$ µm or tool cutting edge outbreaks larger than $d = 100$ µm were set as tool life criteria. Cutting process data in terms of process forces was measured using a three-component piezoelectric dynamometer Kistler 9255C, Kistler Instrumente AG, Winterthur, Switzerland. For each coated tool variant two cutting tests until the end of tool service life were carried out. Moreover, in order to analyze the tool wear progress, additional cutting tests until cutting lengths $l_c = 100$ m and $l_c = 500$ m were carried out.

2.4. Extended tool wear analysis

After cutting tests, the wear behavior and underlying wear mechanisms of the cutting inserts were analyzed in detail using Desktop SEM Phenom XL, Thermo Fischer Scientific, Eindhoven, Netherlands. Additionally, flank face of the inserts was analyzed using energy dispersive spectroscopy (EDX) mappings. In order to bring qualitative observations from analysis of EDX maps into a quantitative information, an algorithm based on OpenCV© computer vision libraries for image segmentation and analysis was developed in Python© programming language. The algorithm was designed to identify the tool wear features in EDX maps, generate segmented images and lastly quantify the identified features in segmented images using pixel counting, as exemplarily shown in Fig. 2.

Here three main tool wear features, coating, exposed substrate and workpiece material adhesions on the tool surface were defined. The coating was included as tool wear feature as it represented the tool area where the coating was subjected to wear, but remained largely intact. The segmented images show the calculated area for coating, exposed substrate and workpiece material adhesions as well as their individual percentual contributions to the total calculated wear area A_w. The total calculated wear area was defined as the sum of the calculated area for coating, exposed substrate and workpiece material within the ROI. For rake face of the inserts, the algorithm was programmed to analyze the grey scale SEM images. Both algorithms were iteratively fine-tuned so that $n_{pixel} > 90$ % of the total identified pixels relevant to tool wear were assigned to either of the three defined wear features. Moreover, CLSM was used to measure the length K_L, width K_B and depth K_T of crater wear on rake face of cutting inserts.

3. Results and discussion

3.1. Coating and compound properties

Table 2 shows the overall coating thickness, chemical composition of the top layer, average line roughness Ra and adhesion strength class HF of the coatings. The chemical composition of the TiAlCrSiN interlayer for bilayer variant was similar as that of monolayer TiAlCrSiN. For TiAlCrSiON top layer, the Cr and Si content reduced due to poisoning of corresponding targets installed at dcMS cathodes. Moreover, incorporation of oxygen came at the expense of nitrogen and in an increased non-metallic content of the coating.

SEM cross-section images exhibited similar columnar morphology for both coatings, see Fig. 3. Fine vertical columns grew together in form of large clusters resulting in cauli-flower like surface morphology as common for columnar PVD coatings.

Fig. 4 shows the results from elastic-plastic deformation behavior of coatings at varying temperatures characterized by nanoindentation measurements. The plastic work percentage η_{plast} represents percentual contribution of plastic deformation work W_{plast} to the total work W_{total} during indentation. W_{total} is calculated as sum of elastic reverse

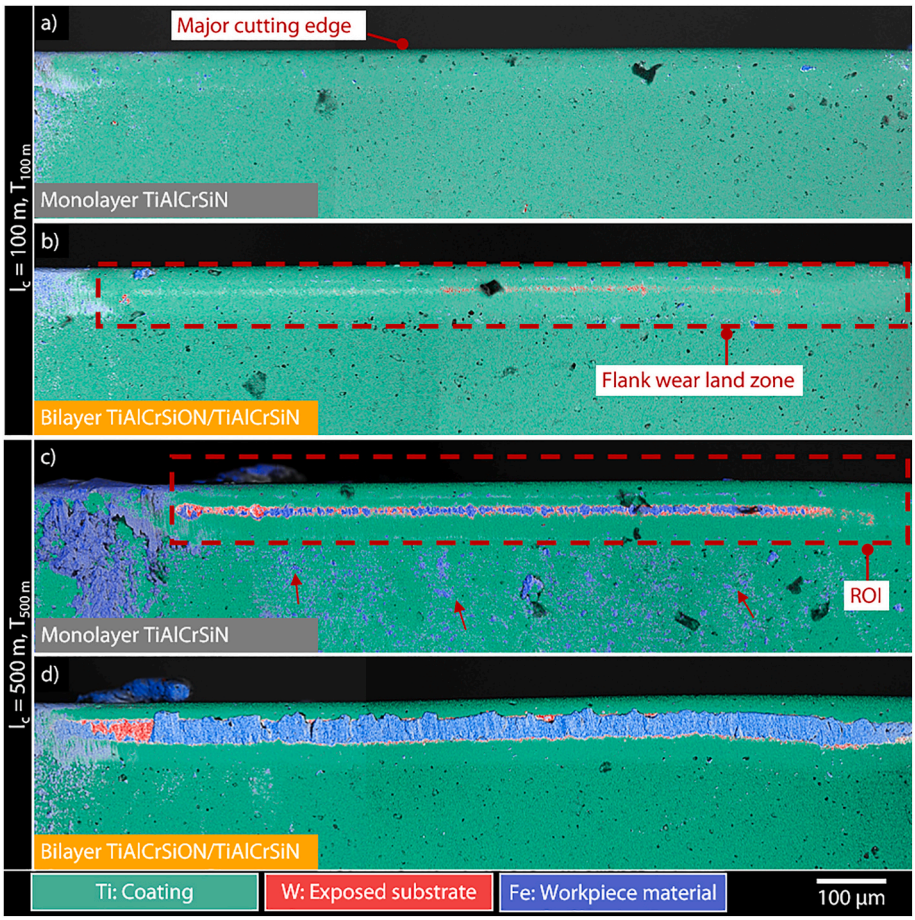

Fig. 8. EDX maps of flank face of TiAlCrSiN and TiAlCrSiON/TiAlCrSiN coated cutting inserts after cutting length (a–b) l_c = 100 m and (c–d) l_c = 500 m.

deformation work W_{elast} and plastic deformation work W_{plast}. W_{plast} is calculated as area between the loading and unloading segments of the force-displacement curve. W_{elast} is calculated as area under the unloading segment of the force-displacement curve. At T = 23 °C monolayer showed a higher average H_{IT} = (29.4 ± 2.4) GPa compared to bilayer variant with average H_{IT} = (26.5 ± 1.8) GPa. As discussed in Ref. [21], incorporation of oxygen may led to an increased amorphous content in the coating and reduce indentation hardness H_{IT}. A similar trend was also observed for indentation modulus E_{IT} and plastic work percentage η_{plast} at T = 23 °C. An increased η_{plast} combined with a lower H_{IT} for bilayer TiAlCrSiON/TiAlCrSiN means an increased coating deformation in terms of maximum indentation depth h_{max} and reduced elastic recovery of the coating compared to monolayer TiAlCrSiN. As the measurement temperature increased, both coatings showed a gradual decrease in H_{IT}. At T = 600 °C, the coatings displayed an overall reduction of $\Delta H_{IT} \approx 5.5$ GPa compared to initial H_{IT} values at T = 23 °C. However, the monolayer TiAlCrSiN consistently showed higher H_{IT} values compared to bilayer variant as the measurement temperatures increased, see Fig. 4a). Monolayer variant showed a slight increase in E_{IT} with measurement temperature, whereas bilayer TiAlCrSiON/TiAlCrSiN did not show any significant temperature dependent increase in E_{IT}. Hence, monolayer TiAlCrSiN showed better elastic recovery and consequently reduced plastic work percentage η_{plast} compared to bilayer variant at considered measurement temperatures. After cooling down H_{IT}, E_{IT} and η_{plast} values for monolayer TiAlCrSiN returned to its initial values at T = 23 °C before heating. Interestingly, bilayer TiAlCrSiON/-TiAlCrSiN showed increased H_{IT} and E_{IT} values and resultantly reduced η_{plast} after cooling down compared to its initial values. As previously investigated in Ref. [12], TiAlCrSiN and TiAlCrSiON coatings have shown phase stability until T = 1200 °C and oxidation resitance until T = 900 °C. The discussed trends for temperature dependent elastic-plastic deformation behavior of both variants could presumably be attributed to changes in compressive residual stress state of the coatings as a consequence of relaxation effects taking place at higher temperatures. An increase in temperature may reduce the residual stresses of the coating, resulting in an increased coating deformation in terms of indentation depth h and consequently reduced hardness H_{IT} and increased plastic work percentage η_{plast} of the coatings. However, the relaxation effects and resulting change in residual stress state at higher temperatures may also be dependent on non-metallic content of the coating as observed in present case.

3.2. Tool wear and process data

Results of cutting tests for inserts coated with monolayer TiAlCrSiN and bilayer TiAlCrSiON/TiAlCrSiN are shown in Fig. 5. The cutting tests are represented by their test number V whereas additional test series until l_c = 100 m and l_c = 500 m are marked by $T_{100\ m}$ and $T_{500\ m}$, respectively. As the cutting length l_c increased, both variants showed a gradual increase in flank wear land width VB until l_c = 500 m. As compared to bilayer variant, the monolayer variant exhibited a reduced VB until l_c = 300 m. However, the cutting inserts for both coatings went into progressive tool wear phase after l_c = 500 m.

Fig. 6 exemplarily displays the wear progress at flank face and rake face of the inserts as the cutting length increased. The results from other tests were comparable to the ones shown in Fig. 6.

The inserts primarily underwent abrasive wear on tool flank face and crater wear on tool rake face. As the cutting length increased, the area of crater wear increased and eventually reached the minor cutting edge of the insert. This led to chipping and breakage along the minor cutting

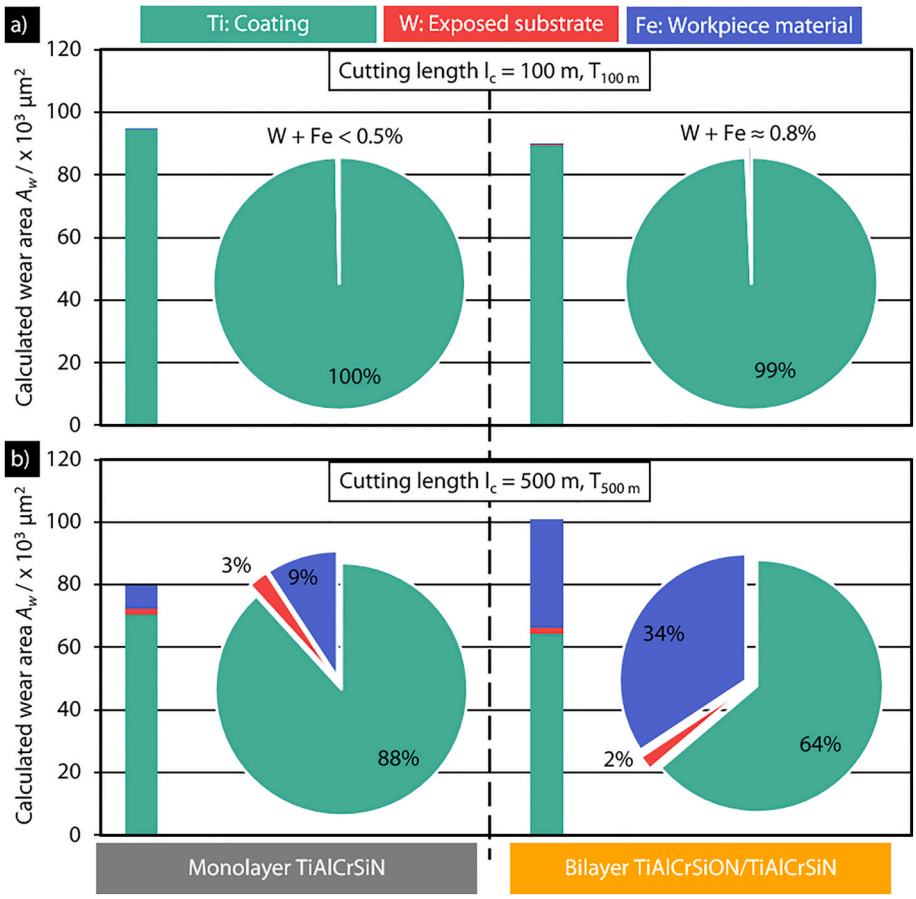

Fig. 9. Quantitative analysis of tool wear features on flank face of TiAlCrSiN and TiAlCrSiON/TiAlCrSiN coated inserts at cutting lengths (a) l_c = 100 m and l_c = 500 m.

edge and an increase in tool load. Resultantly, the flank wear along the major cutting edge accelerated and the cutting inserts went into progressive tool wear phase. The crater wear is known to originate in chip-tool interaction zone at the rake face. The chip flow across the rake face leads to gradual abrasive wear of coating and exposure of cemented carbide substrate. At this stage, the workpiece material adheres on the rake face and may diffuse into the substrate. This diffusion eventually reduces the resistance of the cemented carbide against abrasive wear resulting in crater formation on tool rake face [22]. The process forces for the cutting tests with the inserts in Fig. 6 are shown in Fig. 7. The process forces for the remaining cutting tests were comparable. As the VB increased almost linearly over the cutting length until l_c = 500 m, both variants showed a slight change in cutting force F_c, passive force F_p, feed force F_f and resultant force F_r. As expected, the process forces increased significantly as the cutting inserts went into progressive tool wear mode after l_c = 500 m. Interestingly, all three force components F_c, F_p and F_f and the resultant force F_r consistently showed reduced absolute values for the cutting inserts coated with bilayer TiAlCrSiON/TiAlCrSiN. The reason for this reduction in process forces became apparent during detailed tool wear analysis discussed in next section.

3.3. Qualitative and quantitate analysis of tool wear behavior

Fig. 8 displays EDX maps of flank face of the inserts after l_c = 100 m and l_c = 500 m. The coating is represented in light green color by Ti, tool material or substrate in red by W and adhesions from workpiece material in blue by Fe. Ti, W and Fe were chosen due to their exclusive presence in coating, substrate and workpiece material, respectively. Other elements such as Al, Cr, Si, Mo and Co were ignored as they overlapped with either of the three considered elements in EDX maps. Moreover, qualitative analysis of EDX maps showed no oxidation of investigated coatings in present case. As apparent from EDX maps, the tool damage on flank face started initially with abrasive wear of the coating resulting in development of flank wear land zone. The length of the flank wear land zone was limited by the end of chip flow zone along the main cutting edge on rake face. The abrasive wear of the coating on flank face increased with the cutting length l_c leading to exposure of substrate material. Within the flank wear land zone, the workpiece material mainly adhered to the exposed substrate. The flank wear land zone was followed by extensive adhesion of the workpiece material on the tool surface as expected in case of dry turning processes. As compared to monolayer TiAlCrSiN, bilayer TiAlCrSiON/TiAlCrSiN showed a reduced resistance to abrasive wear and resultantly increased workpiece material adhesion on exposed substrate surface. This could be attributed to the lower temperature dependent hardness H_{IT} of the bilayer variant. However, below the flank land wear zone, the workpiece material showed a reduced adhesion tendency to bilayer coating as evident in Fig. 8c) and d). In order to bring these qualitative observations on tool wear into quantitate information, the EDX maps were evaluated using the image analysis algorithm explained in section 2.4. For this purpose, region of interest (ROI) of h ≈ 150 µm in height around the major cutting edge and length dependent on the end the of flank wear land zone was selected, as exemplarily marked in Fig. 8c). The ROI was divided around the major cutting edge in a way that A_{ROI} ≈ 60 % covered the area below the major cutting edge. In order to maintain a consistent ROI for the analyzed cutting inserts, any workpiece material adhesions on the major cutting edge visible from the flank face were also included in the analysis.

Fig. 9 shows the quantified information on the identified features relevant for quantitative tool wear analysis. The calculated wear area

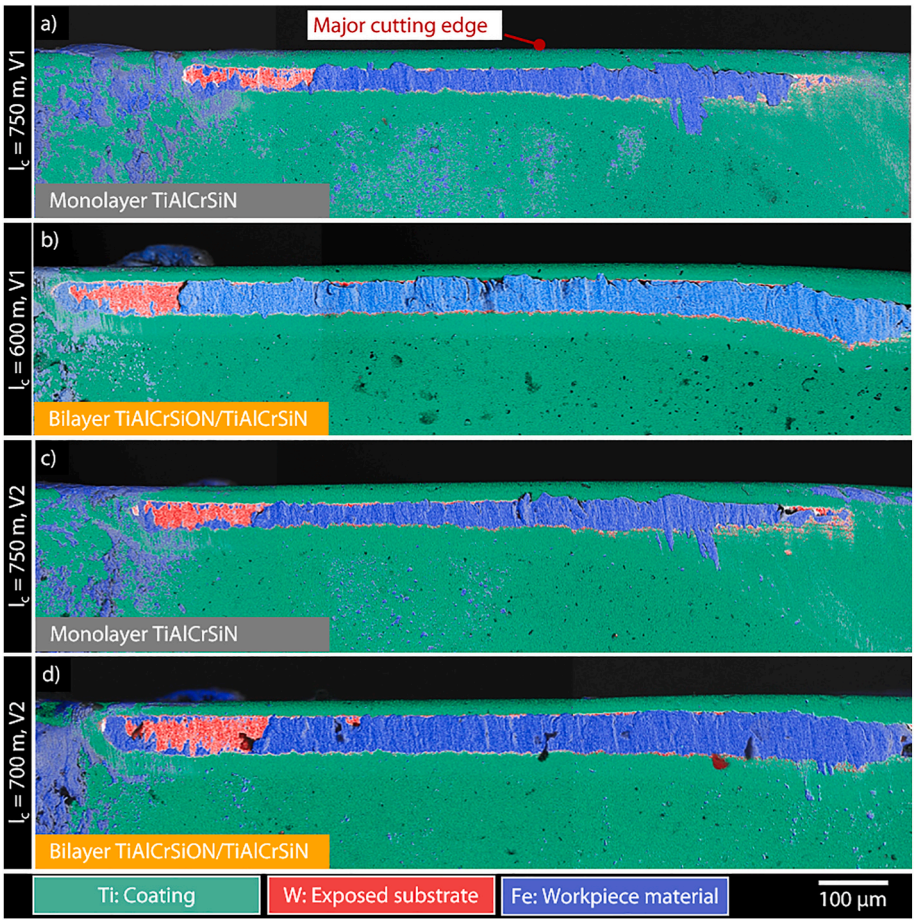

Fig. 10. EDX maps of flank face of (a&c) TiAlCrSiN and (b&d) TiAlCrSiON/TiAlCrSiN coated cutting inserts at the end of tool service life.

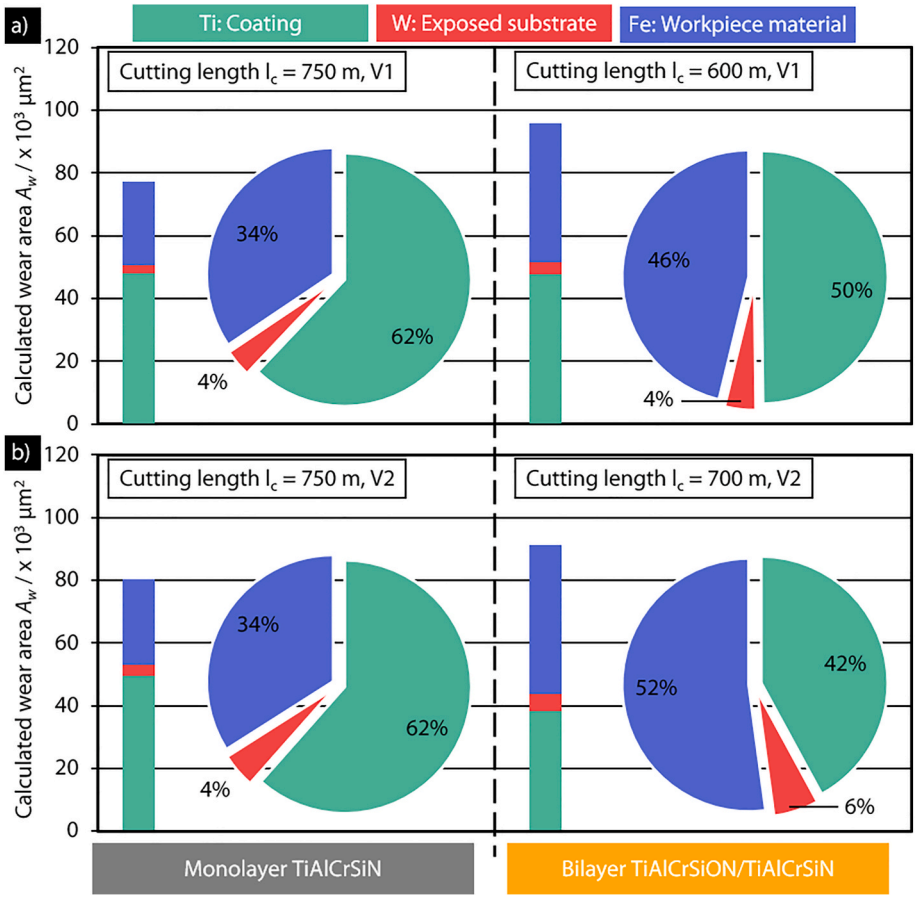

Fig. 11. Quantitative analysis of tool wear features on flank face of (a&c) TiAlCrSiN and (b&d) TiAlCrSiON/TiAlCrSiN coated cutting inserts at the end of tool service life.

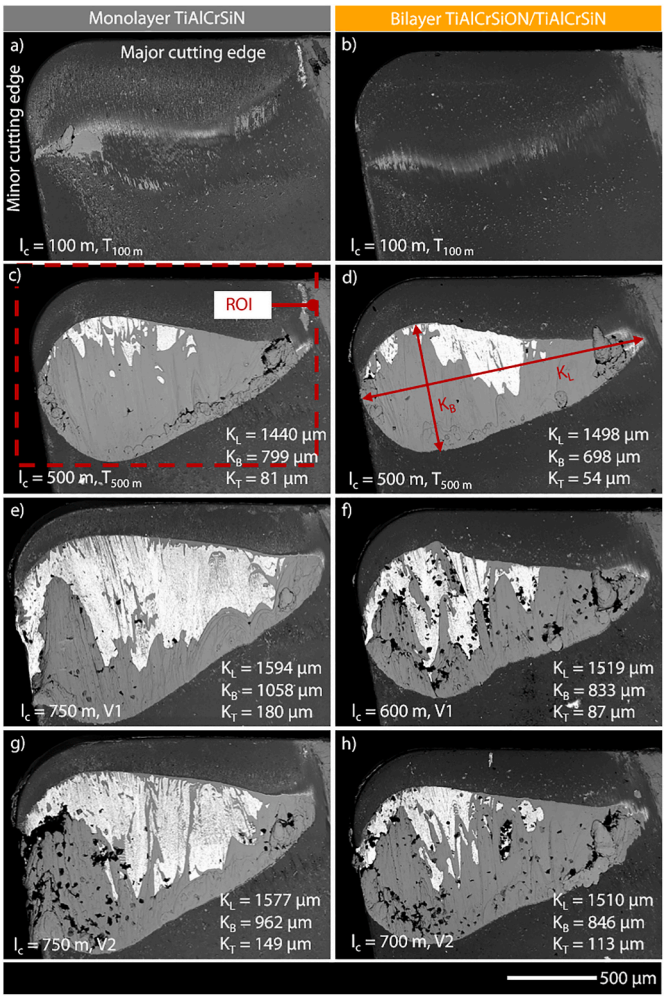

Fig. 12. SEM images of rake face for TiAlCrSiN and TiAlCrSiON/TiAlCrSiN coated cutting inserts at cutting lengths (a,b) l_c = 100 m, (c,d) l_c = 500 m and (e–h) at end of tool service life.

represents the area belonging to coating, exposed substrate and workpiece material adhesions within the ROI. The pie charts show the percentual contribution of coating, exposed substrate and workpiece adhesion to the calculated wear area A_w. As qualitatively observed from EDX maps, the quantitative results exhibited a larger calculated wear area A_w and increased combined contribution from exposed substrate and workpiece material adhesions at l_c = 500 m for bilayer variant compared to monolayer variant.

Fig. 10 shows EDX maps of flank face of the cutting inserts at the end of their service life. Again, the inserts coated with bilayer variant showed an increased flank wear land zone compared to the ones coated with monolayer TiAlCrSiN. Moreover, the reduced abrasion resistance of bilayer variant resulted in increased substrate exposure combined with workpiece material adhesion.

The quantified information on qualitative tool wear analysis at the end of tool service life is shown in Fig. 11. The quantitative analysis resonates well with the qualitative observations. The cutting inserts with monolayer TiAlCrSiN showed a reduced overall calculated wear area A_w and higher contribution from coating inside A_w as compared to inserts coated with bilayer variant. Interestingly, the inserts with monolayer TiAlCrSiN showed similar percentual contributions from tool wear features to the A_w. Due to the lower abrasive wear resistance, the bilayer variant exhibited an increased joint contribution from exposed substrate and workpiece material adhesions to A_w.

SEM images of rake face of the cutting inserts along with the measured length K_L, width K_B and depth K_T of crater wear are shown in Fig. 12. As confirmed by EDX-analysis, coating is represented in dark grey, workpiece material adhesions in light grey and exposed substrate in white color.

The cutting inserts with bilayer TiAlCrSiON/TiAlCrSiN displayed a higher resistance against crater wear. As compared to monolayer TiAlCrSiN, the bilayer TiAlCrSiON/TiAlCrSiN reduced the width K_B and depth K_T of crater wear on the rake face of the inserts. This could be attributed to reduced adhesion tendency of workpiece material to oxynitride top layer of bilayer variant. As apparent from the initial stage of crater development at l_c = 100 m, see Fig. 12a) and b), cutting inserts with bilayer TiAlCrSiON/TiAlCrSiN exhibited reduced adhesion of workpiece material in chip-tool interaction zone. This may lead to reduced friction between the chip and tool surface to increase the crater wear resistance for TiAlCrSiON/TiAlCrSiN coated cutting inserts. The quantitative tool wear analysis on rake face of the inserts mirror the observations from qualitative analysis, see Figs. 13 and 14.

ROI for analysis on rake face for each cutting insert was chosen in a way that the complete crater wear area as well as the major and minor cutting edges were included, as shown exemplarily in Fig. 12c). At l_c = 100 m and l_c = 500 m, inserts with monolayer coating exhibited comparable calculated wear area A_w to the corresponding inserts with bilayer coating. However, an increased workpiece material adhesion was observed for the inserts coated with monolayer TiAlCrSiN.

Depending on the coating, the cutting inserts at the end of their service life also displayed different calculated wear areas A_w. This also correlates well with qualitative analysis and crater wear measurements as the bilayer TiAlCrSiON/TiAlCrSiN resulted in an increased resistance of coated inserts against crater wear. Furthermore, the effect of oxynitride top layer on improvement of chip-tool tribological interaction and reduction of crater wear correlates well with the measured process forces. As compared to monolayer TiAlCrSiN, bilayer TiAlCrSiON/TiAlCrSiN coating resulted in lower process forces during the cutting process, see Fig. 7. This reduction in process forces is attributed to the improved tribological behavior and increased crater wear resistance of the cutting inserts coated with bilayer TiAlCrSiON/TiAlCrSiN.

4. Conclusion

Wear behavior of cemented carbide inserts coated with monolayer TiAlCrSiN and bilayer TiAlCrSiON/TiAlCrSiN for high performance turning of 42CrMo4+QT alloy steel was investigated using an extended qualitative and quantitative tool wear analysis approach. Although the cutting inserts showed a comparable performance in terms of tool service life, the extended tool wear analysis approach disclosed the difference in wear behavior of the coated inserts. On tool flank face, abrasive wear of the coating was followed by substrate exposure and workpiece material adhesion to the exposed substrate. Here, monolayer TiAlCrSiN, due to its higher temperature-dependent indentation hardness H_{IT}, displayed increased resistance to abrasive wear. However, the oxynitride top layer for bilayer variant reduced the adhesion tendency of workpiece material to the tool rake face and resultantly improved the resistance of the cutting inserts against crater wear. Hence, despite the reduced abrasive wear resistance of bilayer TiAlCrSiON/TiAlCrSiN the corresponding cutting inserts showed comparable performance to the ones coated with monolayer TiAlCrSiN. Moreover, the qualitative observations on tool wear behavior were validated with quantitative tool wear analysis data and measured process forces. The findings highlight the importance of the presented extended tool wear analysis approach to qualitatively as well as quantitatively investigate the wear behavior of PVD coated cutting tools for an improved understanding of correlations between tool wear and cutting process data. Moreover, the detailed quantified information on tool wear behavior and underlying wear mechanisms may contribute, in future, to the development of accurate tool wear prediction models required for qualification of PVD coated cutting tools.

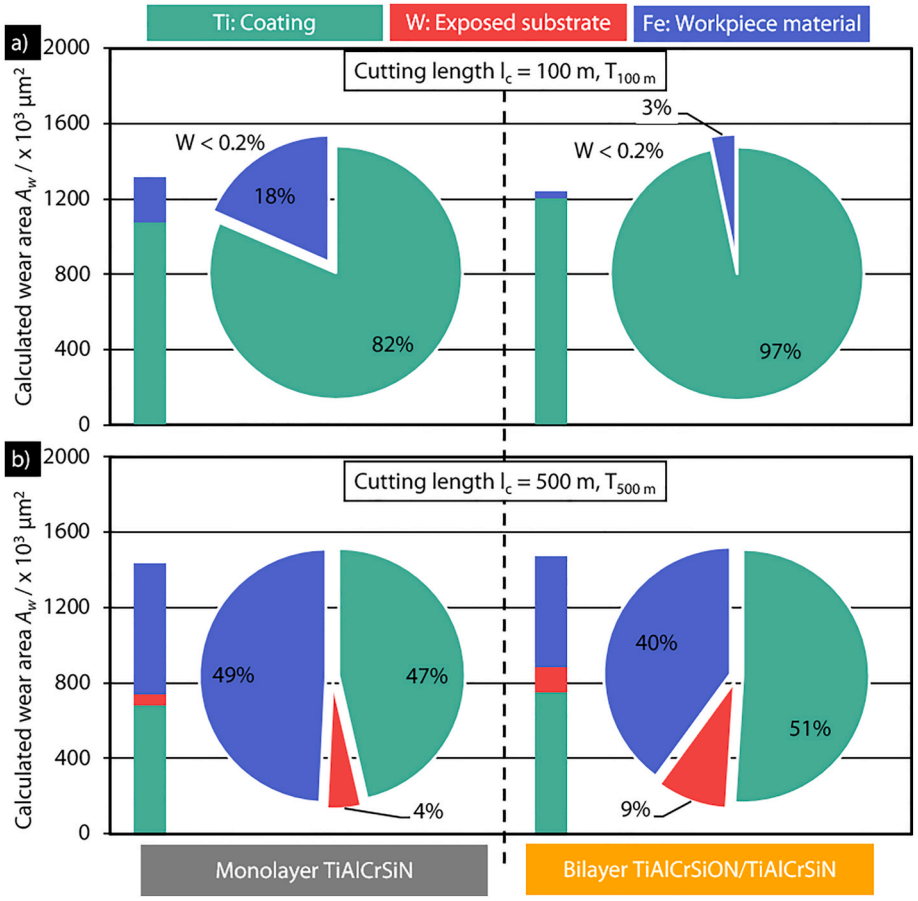

Fig. 13. Quantitative analysis of tool wear features on rake face of TiAlCrSiN and TiAlCrSiON/TiAlCrSiN coated inserts at cutting lengths (a) l_c = 100 m and l_c = 500 m.

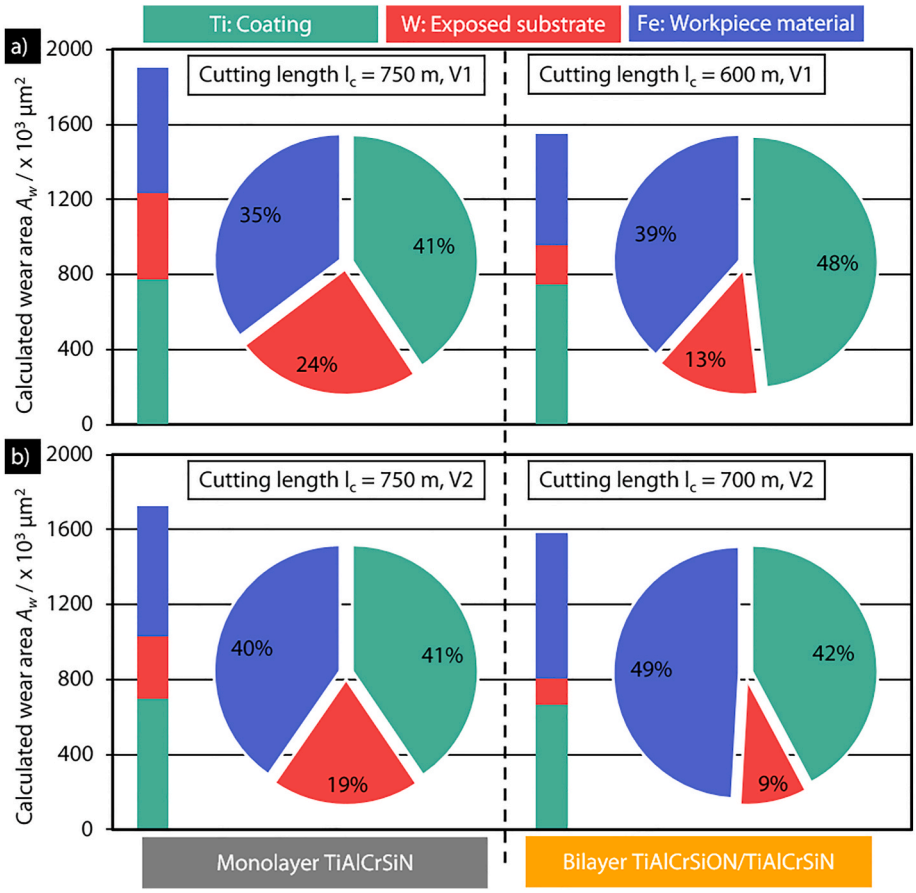

Fig. 14. Quantitative analysis of tool wear features on rake face of (a&c) TiAlCrSiN and (b&d) TiAlCrSiON/TiAlCrSiN coated cutting inserts at the end of tool service life.

CRediT authorship contribution statement

K. Bobzin: Writing – review & editing, Supervision, Resources, Project administration, Funding acquisition, Conceptualization. **C. Kalscheuer:** Writing – review & editing, Supervision, Project administration, Funding acquisition, Conceptualization. **M. Tayyab:** Writing – original draft, Visualization, Methodology, Investigation, Formal analysis, Conceptualization. **T. Bergs:** Writing – review & editing, Supervision, Resources, Project administration, Funding acquisition, Conceptualization. **M. Meurer:** Writing – review & editing, Supervision, Project administration, Funding acquisition, Conceptualization. **M. Abouridouane:** Writing – review & editing, Visualization, Methodology, Investigation, Formal analysis, Conceptualization.

Declaration of competing interest

The authors declare that they have no known competing financial interests or personal relationships that could have appeared to influence the work reported in this paper.

Acknowledgement

The authors gratefully acknowledge the financial support of the German Research Foundation, Deutsche Forschungsgemeinschaft (DFG), within the project 521280523.

Data availability

Data will be made available on request.

References

[1] A. Inspektor, P.A. Salvador, Architecture of PVD coatings for metalcutting applications: a review, Surf. Coating. Technol. 257 (2014) 138–153, https://doi.org/10.1016/j.surfcoat.2014.08.068.
[2] S. Vepřek, S. Reiprich, L. Shizhi, Superhard nanocrystalline composite materials: the TiN/Si3N4 system, Appl. Phys. Lett. 66 (1995) 2640–2642, https://doi.org/10.1063/1.113110.
[3] E. Huber, S. Hofmann, Oxidation behaviour of chromium-based nitride coatings, Surf. Coating. Technol. 68–69 (1994) 64–69, https://doi.org/10.1016/0257-8972(94)90139-2.
[4] N. Jiang, Y. Shen, Y.-W. Mai, T. Chan, S.C. Tung, Nanocomposite Ti–Si–N films deposited by reactive unbalanced magnetron sputtering at room temperature, Mater. Sci. Eng., B 106 (2004) 163–171, https://doi.org/10.1016/j.mseb.2003.09.033.
[5] H.-D. Männling, D. Patil, K. Moto, M. Jilek, S. Veprek, Thermal stability of superhard nanocomposite coatings consisting of immiscible nitrides, Surf. Coating. Technol. 146–147 (2001) 263–267, https://doi.org/10.1016/S0257-8972(01)01474-8.
[6] T. Chen, Z. Xie, F. Gong, Z. Luo, Z. Yang, Correlation between microstructure evolution and high temperature properties of TiAlSiN hard coatings with different Si and Al content, Appl. Surf. Sci. 314 (2014) 735–745, https://doi.org/10.1016/j.apsusc.2014.06.057.
[7] C.R. Das, M. Rangwala, A. Ghosh, Effect of Si contents on microstructure and mechanical characteristics of TiAlSiN thin film deposited by HiPIMS using different Ti Si target compositions, Surf. Coating. Technol. 476 (2024) 130212, https://doi.org/10.1016/j.surfcoat.2023.130212.
[8] W. Tillmann, M. Dildrop, Influence of Si content on mechanical and tribological properties of TiAlSiN PVD coatings at elevated temperatures, Surf. Coating. Technol. 321 (2017) 448–454, https://doi.org/10.1016/j.surfcoat.2017.05.014.
[9] S. Vepřek, The search for novel, superhard materials, J. Vac. Sci. Technol. A: Vacuum, Surfaces, and Films 17 (1999) 2401–2420, https://doi.org/10.1116/1.581977.
[10] S.L. Soo, S.A. Khan, D.K. Aspinwall, P. Harden, A.L. Mantle, G. Kappmeyer, D. Pearson, R. M'Saoubi, High speed turning of Inconel 718 using PVD-coated PCBN tools, CIRP Annals 65 (2016) 89–92, https://doi.org/10.1016/j.cirp.2016.04.044.
[11] Y.-Y. Chang, H.-M. Lai, Wear behavior and cutting performance of CrAlSiN and TiAlSiN hard coatings on cemented carbide cutting tools for Ti alloys, Surf.

Coating. Technol. 259 (2014) 152–158, https://doi.org/10.1016/j.surfcoat.2014.02.015.
[12] K. Bobzin, T. Brögelmann, N.C. Kruppe, M. Carlet, Wear behavior and thermal stability of HPPMS (Al,Ti,Cr,Si)ON, (Al,Ti,Cr,Si)N and (Ti,Al,Cr,Si)N coatings for cutting tools, Surf. Coating. Technol. 385 (2020) 125370, https://doi.org/10.1016/j.surfcoat.2020.125370.
[13] K. Bobzin, T. Brögelmann, N.C. Kruppe, M. Carlet, D.C. Hoffmann, B. Breidenstein, A. Krödel, S. Beblein, HPPMS tool coatings: chip formation and friction, Vakuum Forsch. Praxis 33 (2021) 26–33, https://doi.org/10.1002/vipr.202100765.
[14] W. Sujuan, Z. Tao, D. Wenping, S. Zhanwen, S. To, Analytical modeling and prediction of cutting forces in orthogonal turning: a review, Int. J. Adv. Manuf. Technol. 119 (2022) 1407–1434, https://doi.org/10.1007/s00170-021-08114-y.
[15] Le Wang, C. Yue, X. Liu, M. Li, Y. Xu, S.Y. Liang, Conventional and micro scale finite element modeling for metal cutting process: a review, Chin. J. Aeronaut. 37 (2024) 199–232, https://doi.org/10.1016/j.cja.2023.03.004.
[16] J. Zhang, Y. Zeng, B. Starly, Recurrent neural networks with long term temporal dependencies in machine tool wear diagnosis and prognosis, SN Appl. Sci. 3 (2021), https://doi.org/10.1007/s42452-021-04427-5.
[17] B. Yan, L. Zhu, Y. Dun, Tool wear monitoring of TC4 titanium alloy milling process based on multi-channel signal and time-dependent properties by using deep learning, J. Manuf. Syst. 61 (2021) 495–508, https://doi.org/10.1016/j.jmsy.2021.09.017.
[18] H.J. Tulleken, Grey-box modelling and identification using physical knowledge and bayesian techniques, Automatica 29 (1993) 285–308, https://doi.org/10.1016/0005-1098(93)90124-C.
[19] L. Nägele, M. Meurer, T. Bergs, M. Tayyab, C. Kalscheuer, K. Bobzin, Verbesserte Standzeitprognosen von Werkzeugen durch Greybox-Modelle, Masch.Bau 4 (2024) 26–29, https://doi.org/10.1007/s44029-024-1173-9.
[20] W.C. Oliver, G.M. Pharr, An improved technique for determining hardness and elastic modulus using load and displacement sensing indentation experiments, J. Mater. Res. 7 (1992) 1564–1583, https://doi.org/10.1557/JMR.1992.1564.
[21] K. Bobzin, T. Brögelmann, N.C. Kruppe, M. Carlet, Investigation on the incorporation of oxygen and thermal stability of HPPMS TiAlCrSiON nanolayer coatings, Surf. Coating. Technol. 418 (2021) 127231, https://doi.org/10.1016/j.surfcoat.2021.127231.
[22] F. Klocke, Fertigungsverfahren 1: Zerspanung mit geometrisch bestimmter Schneide, 9. Aufl. 2018, Springer Berlin Heidelberg, Berlin, Heidelberg, 2018. ISBN: 9783662542071.